# On the Observed Relationships between Wintertime Variability in Kuroshio–Oyashio Extension Sea Surface Temperatures and the Atmospheric Circulation over the North Pacific

SAMANTHA M. WILLS AND DAVID W. J. THOMPSON

*Department of Atmospheric Science, Colorado State University, Fort Collins, Colorado*

(Manuscript received 22 May 2017, in final form 29 March 2018)

ABSTRACT

Observational analyses reveal that wintertime variations in sea surface temperatures (SST) in the Kuroshio–Oyashio Extension (KOE) region of the North Pacific are associated with two distinct and robust patterns of atmospheric variability: 1) a pattern that peaks in amplitude approximately 2–3 weeks prior to large KOE SST anomalies and is consistent with atmospheric forcing of the SST field and 2) a very different pattern that lags SST anomalies in the KOE region by approximately a month. The latter pattern is dominated by low sea level pressure anomalies and turbulent heat fluxes directed into the atmosphere over warm SST anomalies and is interpreted as the transient atmospheric response to SST anomalies over the KOE region. The results contribute to a growing body of evidence that suggests variations in SSTs in the midlatitude oceans are capable of significantly influencing the large-scale atmospheric circulation, especially near western boundary currents.

## 1. Introduction

The atmospheric response to *tropical* sea surface temperature (SST) anomalies is robust in both models and observations. In contrast, the atmospheric response to *midlatitude* SST anomalies is relatively subtle and difficult to detect, particularly in observations. That is because in the midlatitudes, air–sea interaction is dominated by atmosphere-to-ocean forcing (e.g., Davis 1976, 1978; Deser and Timlin 1997; Ciasto and Thompson 2004), and the influence of the ocean on the atmosphere is small in comparison to internal atmospheric variability (e.g., Palmer and Sun 1985; Barsugli and Battisti 1998; Kushnir et al. 2002). From a thermodynamic perspective, the surface heat fluxes into the atmosphere associated with midlatitude SST anomalies are readily balanced by modest changes in the low-level horizontal wind since the horizontal gradients in temperature are relatively large (e.g., Hoskins and Karoly 1981). As such, the theoretical response to midlatitude SST anomalies is not only weak, but also largely confined to the lower troposphere.

Recent advancements in the resolution of satellite observations and numerical models over the past decade have provided new evidence that suggests the midlatitude ocean has a more important influence on the atmospheric circulation than previously thought, particularly in regions of large horizontal SST gradients. Observations of wind stress curl and divergence from the QuikSCAT satellite radar scatterometer (e.g., Chelton et al. 2001) indicate that surface air blowing across an ocean front (or a region of large horizontal SST gradients) accelerates the surface flow, leading to patterns of convergence and divergence at the surface (e.g., O'Neill et al. 2003; Nonaka and Xie 2003; Chelton et al. 2004; Chelton and Xie 2010). Observational and numerical studies have shown that the *climatological-mean* SST gradients associated with the major western boundary currents are capable of forcing vertical motion (i.e., through changes in the near-surface wind field) well into the free troposphere (e.g., Minobe et al. 2008, 2010), thus influencing the strength and position of the extratropical storm tracks (e.g., Nakamura et al. 2008; Sampe et al. 2010; Small et al. 2014; Piazza et al. 2016).

A growing body of work suggests that *temporal variations* in midlatitude SSTs can also have a significant impact on the atmospheric circulation. For example, observational and numerical studies have shown that

*Corresponding author*: Samantha M. Wills, smwills@atmos.colostate.edu

DOI: 10.1175/JCLI-D-17-0343.1

meridional shifts in the locations of the Kuroshio–Oyashio Extension and Gulf Stream Extension fronts are significantly linked to variations in the large-scale atmospheric circulation on intraseasonal, interannual, and decadal time scales (e.g., Frankignoul et al. 2011; Czaja and Blunt 2011; Taguchi et al. 2012; Kwon and Joyce 2013; Sheldon and Czaja 2014; Smirnov et al. 2015; Révelard et al. 2016). Révelard et al. (2016) found a coherent response to decadal fluctuations in the Kuroshio Extension during the cold season in observational analyses of ERA-Interim during the 1979–2012 time period. Taguchi et al. (2012) argued that SST anomalies in the subarctic frontal zone precede the development of an anomalous circulation pattern reminiscent of the Pacific–North American pattern. An observational study by Frankignoul et al. (2011) indicated that a northward shift in the Oyashio Extension front precedes the development of circulation anomalies reminiscent of the North Pacific Oscillation. In a numerical experiment by Smirnov et al. (2015), a run with a high-resolution atmospheric general circulation model suggested that positive SST anomalies over the Kuroshio–Oyashio Extension (associated with a northward shift in the Oyashio Extension) lead changes in upward vertical motion by several weeks, consistent with studies that have linked anomalously warm SSTs in the Gulf Stream region to vertical motion in the warm sector of extratropical storms (e.g., Czaja and Blunt 2011; Sheldon and Czaja 2014). Both numerical (e.g., Brayshaw et al. 2008; Michel and Rivieré 2014) and observational (e.g., Nakamura and Yamane 2010; O'Reilly and Czaja 2015) studies have also indicated that variations in midlatitude SST gradients are capable of influencing the amplitudes and locations of the storms tracks, where stronger (weaker) midlatitude SST gradients lead to stronger (weaker) and more poleward (equatorward) shifted storm tracks.

The purpose of this study is to explore the observational evidence for midlatitude air–sea interaction over the Kuroshio–Oyashio Extension (KOE) region using lead/lag regressions based on daily-mean data. The study is the companion paper for our recent analysis of the Gulf Stream region (Wills et al. 2016). Unlike the Gulf Stream, the extensions of the Kuroshio–Oyashio currents expand into the open ocean and are not as constrained by land barriers. The North Atlantic and Pacific sectors are also subject to different patterns of climate variability, such as the North Atlantic Oscillation in the North Atlantic sector and ENSO and the Pacific–North American pattern in the North Pacific sector. Hence, it is not clear a priori whether the lead–lag relationships between the atmospheric circulation and SSTs in the western boundary current regions will be similar in the two sectors. A key result of the current study is that—as is the case with SST anomalies in the North Atlantic—SST anomalies in the KOE are associated with two distinct and seemingly independent patterns of atmospheric variability: 1) a pattern that leads the SST field and is consistent with atmospheric forcing of the ocean and 2) a pattern that lags the SST field and may be interpreted as the atmospheric response to midlatitude ocean forcing. The most robust component of the lagged response over both ocean basins is anomalous low surface pressure centered over the warm SST anomalies. Section 2 provides a description of the data. Section 3 explores the observed lead–lag relationships between the atmospheric circulation and SSTs in the KOE. Section 4 compares the KOE results with results based on SST anomalies in the Gulf Stream extension from the companion paper (Wills et al. 2016), and conclusions are provided in section 5.

## 2. Data

The observational analyses are based on daily-mean output from the ERA-Interim reanalyses examined here on a 1.5°-resolution grid over the 35-yr period 1979–2013 (e.g., Dee et al. 2011; https://apps.ecmwf.int/datasets/data/interim-full-daily). To remove the influence of trends on the results, the data were detrended by removing the linear fit from the daily-mean time series at each grid point. Anomalies in SST, potential temperature $\theta$, wind $v$, surface turbulent heat flux THFLX (i.e., sensible + latent heat flux), and geopotential height $Z$ were formed by removing the long-term mean seasonal cycle from the data at all grid points. The long-term mean seasonal cycle is found by averaging all 35 years of the data record as a function of calendar day. Note that, throughout this study, sea level pressure SLP is expressed as geopotential height at 1000 hPa $Z_{1000}$, and THFLX anomalies are positive downward (i.e., positive THFLX anomalies are directed from the atmosphere into the ocean). Apart from the removal of the seasonal cycle and the detrending, the data are not filtered in any other way in the analyses. The statistical significance of key results is shown in Fig. 4, and details of the significance test are provided in the caption.

## 3. Observed lead–lag relationships

### a. Regressions based on KOE SST anomalies

To provide context for the analyses, we show in Fig. 1 a brief synopsis of the winter mean (December–February) circulation and SST field over the North

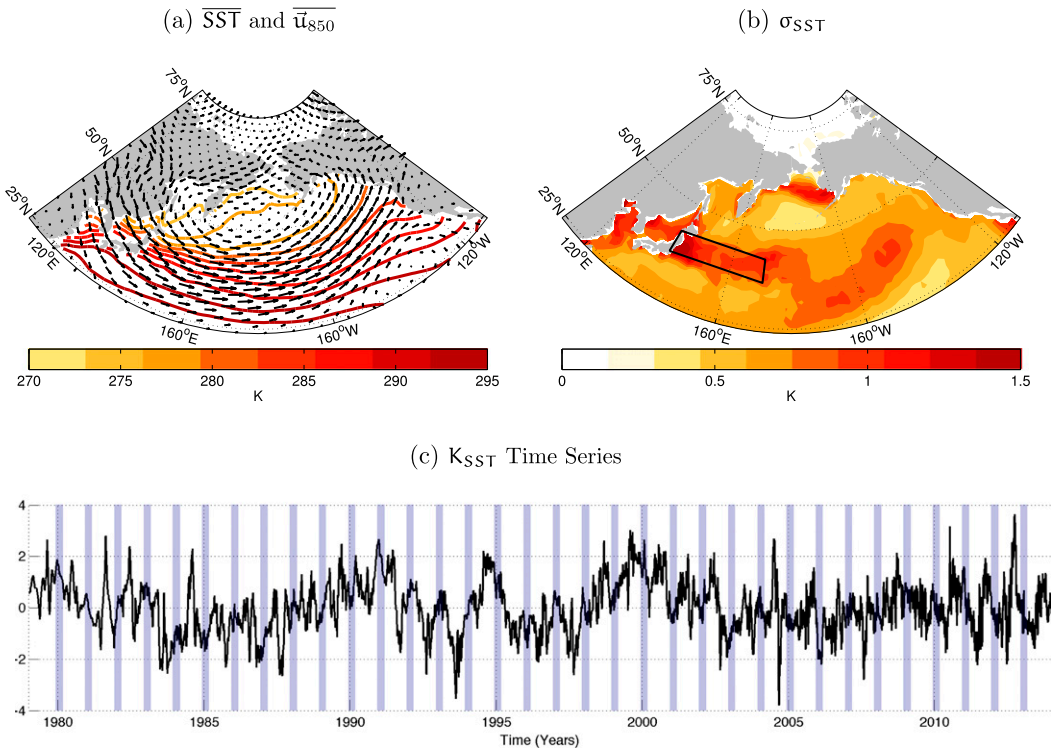


FIG. 1. Climatological values of North Pacific wintertime (DJF) (a) SST (K; contours) and $\mathbf{u}_{850}$ (m s$^{-1}$; vectors) and (b) standard deviation of the SST anomaly field (K; $\sigma_{SST}$). The boxed region spans 36°–42°N, 140°–171°E and indicates the region used to calculate the $K_{SST}$ index. The largest wind vector corresponds to a maximum wind magnitude of ~13 m s$^{-1}$ (not shown). (c) Time series of the standardized $K_{SST}$ index for all days 1979–2013. The sections shaded by blue bars denote the DJF periods.

Pacific. Figure 1a shows the climatological-mean DJF SST and 850-hPa horizontal wind fields ($\mathbf{u}_{850}$); Fig. 1b shows the associated climatological standard deviation of the daily-mean SST anomaly field. Based on the standard deviation of the SST field, it is evident that there are two primary regions of enhanced SST variability in the North Pacific: one to the east of Japan and one in the southeastern North Pacific. Our primary focus is on the region to the east of Japan (indicated by the box in Fig. 1b), which is associated with variability in the KOE (e.g., Nonaka and Xie 2003; Frankignoul et al. 2011; Smirnov et al. 2015), and is where approximately 40%–60% of SST variability is intrinsic to the ocean (i.e., ~50% of monthly SST variability in the KOE region is not influenced by variations in surface atmospheric temperature, or atmosphere-to-ocean forcing) (e.g., Smirnov et al. 2014). The second region of large SST variance (centered near 160°W) is linked to the extratropical atmospheric response to ENSO (e.g., Alexander 1992; Cayan 1992; Diaz et al. 2001) and is not the focus of the current study. The potential contamination of our results by ENSO variability is discussed later in this section.

We investigate the statistical covariability between KOE SSTs and the atmospheric circulation using lead/lag analysis, similar to the statistical technique used in Wills et al. (2016). To capture the SST variability associated with the KOE (i.e., the variance maximum to the east of Japan in Fig. 1b), we create a time series of daily-mean SST anomalies averaged over all grid points in the region 36°–42°N, 140°–171°E (indicated by the box in Fig. 1b). The index (hereinafter $K_{SST}$) is standardized so that it has a mean of zero and standard deviation of one, where positive values of the index correspond to positive SST anomalies in the KOE region, and vice versa. Note that—like the definition of the Gulf Stream region in Wills et al. (2016)—the results are not sensitive to the specific domain used to define the KOE region. The standardized $K_{SST}$ time series is shown in Fig. 1c.

To analyze the relationships between KOE SST anomalies and the anomalous atmospheric circulation, we regressed various atmospheric fields against the $K_{SST}$ index on daily-mean time scales at lags spanning from −30 to +30 days. By construction, the $K_{SST}$ index is always centered within the 90-day period from 1 December to 28 February (i.e., periods highlighted by blue

bars in Fig. 1c), and negative (positive) lags indicate results where the fields being regressed precede (follow) the largest KOE SST anomalies. Hence, at a lag of −30 days (+30 days), the fields being regressed are centered on the 90-day period from 1 November to 29 January (31 December–30 March). The statistical significance of the SLP anomalies at lags of −30 and +30 days is also calculated to assess the robustness of the SLP regression patterns at negative and positive lags (Fig. 4).

The lag regressions in the left column of Fig. 2 highlight the evolution of the anomalous surface atmospheric circulation associated with SST anomalies in the KOE region on daily-mean time scales. Regression coefficients of SST (shading) and SLP (contours) are shown every 15 days between lags of −30 and +30 days. As per the definition of the $K_{SST}$ index, anomalously warm SSTs peak in amplitude over the KOE region at a lag of zero days, and the results show strong persistence in the anomalous SST field through all lags (consistent with the large heat capacity of the ocean). Based on the regressions at negative lags (i.e., when the fields *precede* the largest KOE SST anomalies), it is evident that the warmest SST anomalies are associated with positive SLP anomalies (which peak in amplitude at a lag of −20 days; not shown) that span much of the North Pacific basin, such that the anomalous surface atmospheric circulation inferred from the top-left panel of Fig. 2 acts on the climatological-mean SST gradient (i.e., Fig. 1a) to advect anomalously warm air from the east-southeast over the KOE region. As observed for the Gulf Stream in Wills et al. (2016) and documented in previous literature (e.g., Deser and Timlin 1997; Kushnir et al. 2002; Ciasto and Thompson 2004), this result is consistent with atmospheric forcing of the SST field. Lag regressions of surface turbulent heat flux anomalies onto the $K_{SST}$ index (Fig. 3; shaded) further support this result, as positive (downward) surface turbulent heat flux anomalies at negative lags indicate that the atmosphere is fluxing heat into the ocean prior to the formation of the largest SST anomalies.

The results at positive lags in the left column of Fig. 2 (i.e., when the fields *follow* the largest KOE SST anomalies) indicate that anomalously warm SSTs are followed by a very different pattern of atmospheric circulation anomalies that peak in amplitude at a lag of +30 days (and damp thereafter; lags greater than +30 are not shown). At positive lag, the circulation anomalies are dominated by low SLP anomalies that overlie and extend downstream of the KOE region. The anomalies also include anomalously high SLP centered (approximately) between Alaska and Kamchatka, but as noted below, the high pressure feature is not statistically significant. Importantly, negative (upward) surface turbulent heat flux anomalies are also found over the KOE region at positive lags (Fig. 3), indicating that the ocean is fluxing heat into the overlying atmosphere. This result is consistent with previous findings that suggest a large amount of heat is released to the atmosphere over the Kuroshio–Oyashio confluence region (35°–40°N, 142°–150°E) during periods of anomalously warm SSTs (e.g., Sugimoto and Hanawa 2011; Sugimoto 2014).

The associated structures in the 200-hPa geopotential height and $Z_{200} - Z_{1000}$ fields (right column of Fig. 2) reveal that: 1) the circulation anomalies at negative lag amplify with height and are associated with positive thickness anomalies that extend through the depth of the troposphere and 2) the circulation anomalies at positive lag are associated with much weaker thickness anomalies and are thus relatively confined to lower levels.

The statistical significance of the anomalous circulation patterns at negative and positive lags is shown in Fig. 4. As expected from previous analyses based on pentad and weekly-mean SST data (e.g., Deser and Timlin 1997; Ciasto and Thompson 2004), the most significant SLP and $Z_{200}$ anomalies are found at negative lags (top panels in Fig. 4), when—as discussed above—the atmospheric circulation anomalies are consistent with forcing of the SST field. At positive lag, the low pressure center of action is most significant at the surface. The weak center of high pressure to the north of the KOE region is not statistically significant at any level.

The temporal and spatial resolutions of SSTs prescribed in ERA-Interim are not consistent throughout the entire 1979–2013 time period and this could have an impact on regression analyses based on ERA-Interim SSTs. For example, Masunaga et al. (2015, 2016) found that the location of the near-surface baroclinic zone near the Kuroshio Extension region is highly sensitive to the ''low'' (1979–2001) and ''high'' (2002–2012) resolution periods of ERA-Interim SST, suggesting that long-term changes in the near-surface atmospheric circulation over the western Pacific sector are largely due to improvements in the resolution of SSTs over time. Furthermore, decadal variability in the Pacific decadal oscillation (PDO) can also influence regressions based on data that span the ''regime shift'' in the PDO ~1998/99 (e.g., Mantua et al. 1997; Newman et al. 2016). To test the influence of these factors on our results, we repeated the analyses in Fig. 2 for the 1979–95 and 1996–2013 time periods (Fig. 5, center and right columns, respectively). As evidenced in Fig. 5, the primary features found in the full 35-yr record are reproducible in both halves of the data record.

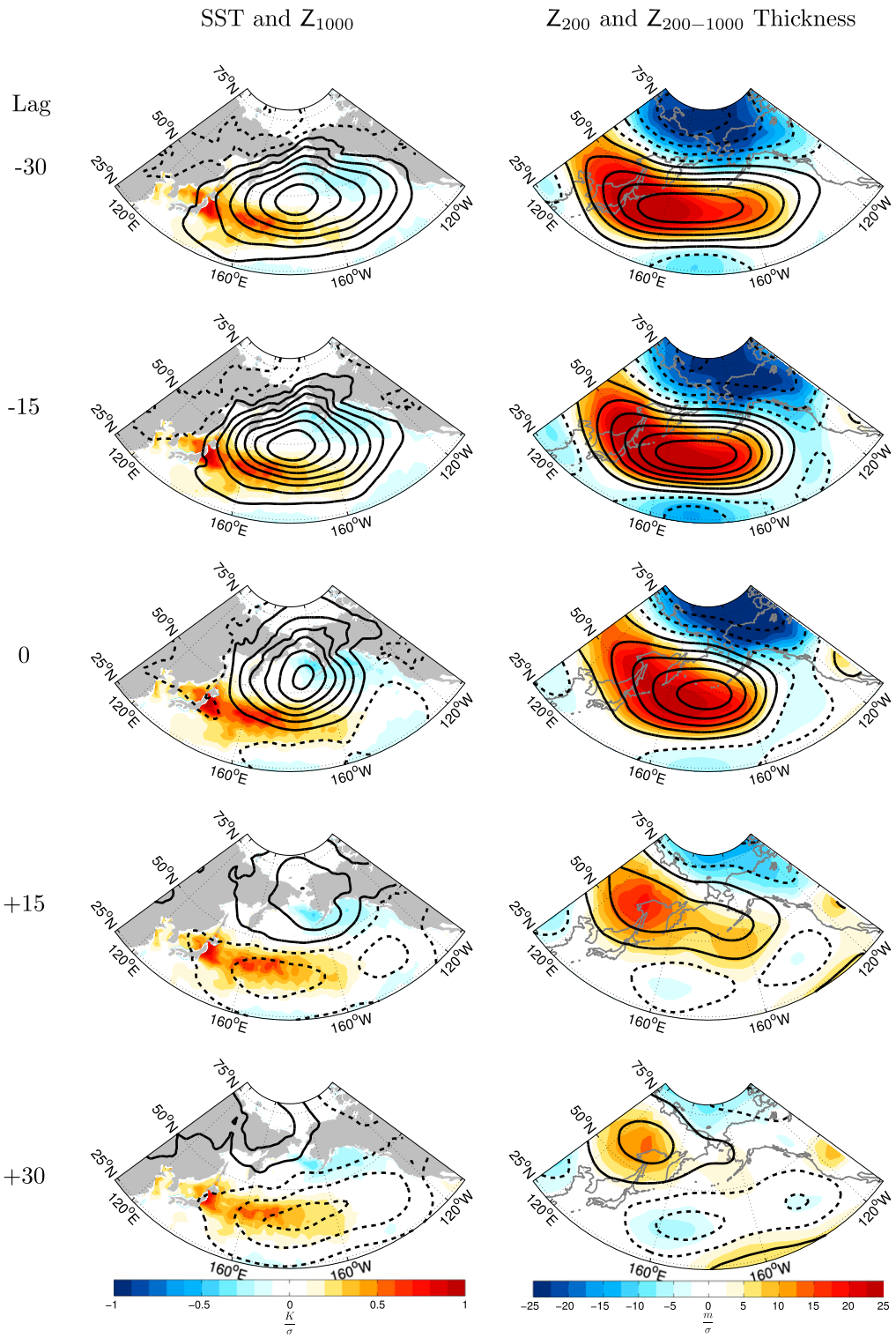


FIG. 2. Wintertime lag regressions of (left) SST and $Z_{1000}$ and (right) $Z_{200}$ and $Z_{200} - Z_{1000}$ ($Z_{200-1000}$) thickness onto the standardized $K_{SST}$ index, with negative (positive) lags denoting $Z_{1000}$/SST and $Z_{200}$/$Z_{200-1000}$ anomalies leading (lagging) $K_{SST}$. The SST and $Z_{200-1000}$ thickness fields are indicated in shading, and the $Z_{1000}$ and $Z_{200}$ fields are indicated by contours, where solid (dashed) lines indicate positive (negative) anomalies. The $Z_{1000}$ contours are spaced at 4-m intervals starting at ±2 m, and $Z_{200}$ contours are spaced at 8-m intervals starting at ±4 m.

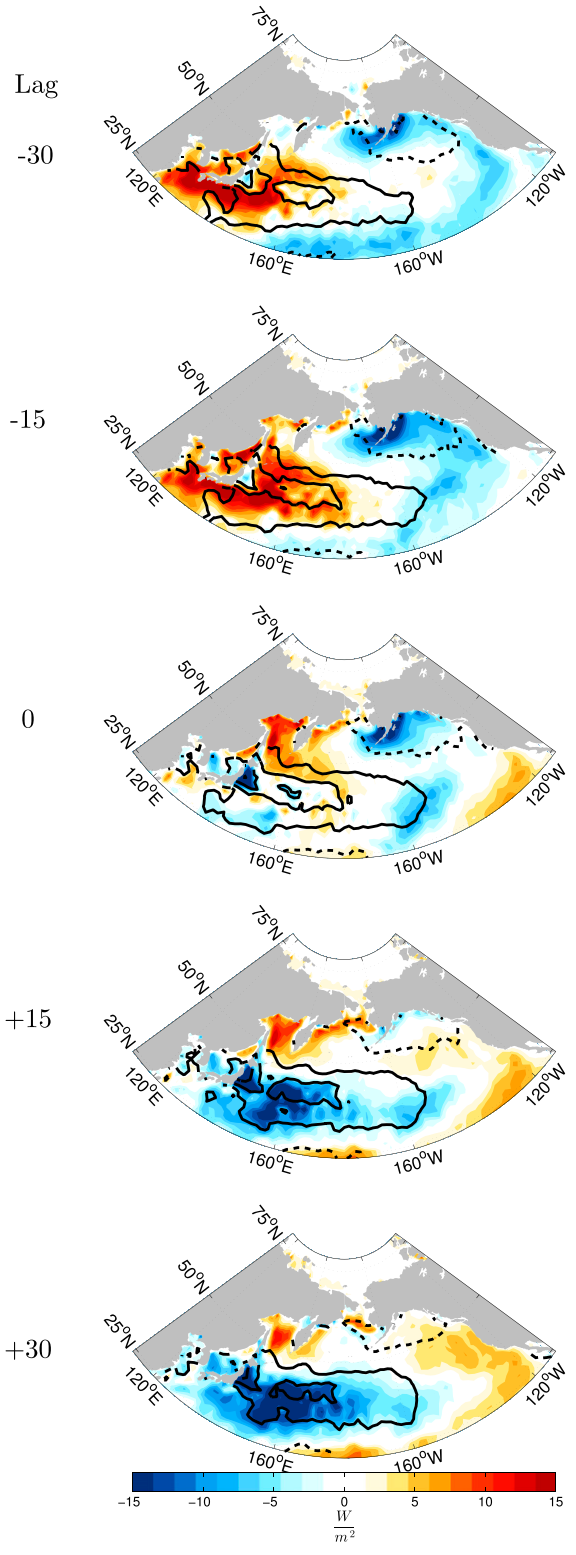


FIG. 3. Wintertime lag regressions of THFLX (shading) and SST (contours) onto the standardized $K_{SST}$ index. SST contours with solid (dashed) lines represent positive (negative) values at an interval spacing of 0.3 K starting at ±0.15 K. Note that THFLX anomalies are positive downward.

### b. Testing for "contamination" by ENSO variability

ENSO has a marked influence on the North Pacific SST field (e.g., Alexander 1992). However, and importantly, it does not contribute to the results shown here. The influence of ENSO was tested as detailed below.

First, we defined ENSO as the standardized low-pass (30 day) filtered time series of daily-mean SST anomalies averaged over the region 6°S–6°N, 171°–120°W (i.e., Niño-3.4). Then, we linearly regressed the ENSO index from the wintertime (November–March) SLP time series at each grid point to form the ENSO-residual SLP data. To determine the optimal lag for the regression, we 1) calculated the amplitude of the North Pacific SLP pattern associated with ENSO as a function of lag (not shown) and 2) identified the time lag when the pattern has maximum amplitude relative to variations in the ENSO index. We then used this lag when calculating the linear fit of the gridded SLP data to ENSO at each grid point over the North Pacific sector. The fits were done for the SLP field lagging the ENSO index by 40 days, but the overall results are largely unchanged for lags ranging from 0 to 90 days.

After removing the ENSO time series from the gridded SLP data, we repeated the analyses in Fig. 2 using the ENSO-residual SLP data. Importantly, removing ENSO from the SLP data does not change the overall patterns or significance of the results in Fig. 2 (results not shown). This is expected, since 1) the correlation between ENSO and the $K_{SST}$ time series is low ($r \sim 0.07$ at lag 0), 2) ENSO explains less than ~10% of the total variance in North Pacific SLP anomalies on daily time scales (not shown), and 3) ENSO is unlikely to contribute to the day-to-day evolution of the North Pacific SLP field, and thus is unlikely to influence the evolution of the SLP anomalies shown in Fig. 2.

### c. Results based on an atmospheric index

Analyses based on the $K_{SST}$ index indicate a significant and distinct pattern of atmospheric circulation anomalies at positive lags (Fig. 2), but it is unclear whether this pattern is dependent on SST anomalies within the KOE region. The SLP pattern at positive lags may be "forced" by the underlying SST anomalies. But it may also simply reflect the evolution of the atmospheric circulation anomalies found at negative lags that would occur independent of the SST field. As done in the companion paper Wills et al. (2016), we tested against the latter possibility by repeating the analyses in Fig. 2, but for regressions based on the expansion coefficient time series of the "atmospheric forcing" pattern (i.e., the pattern of circulation anomalies at negative lags). The atmospheric forcing time series

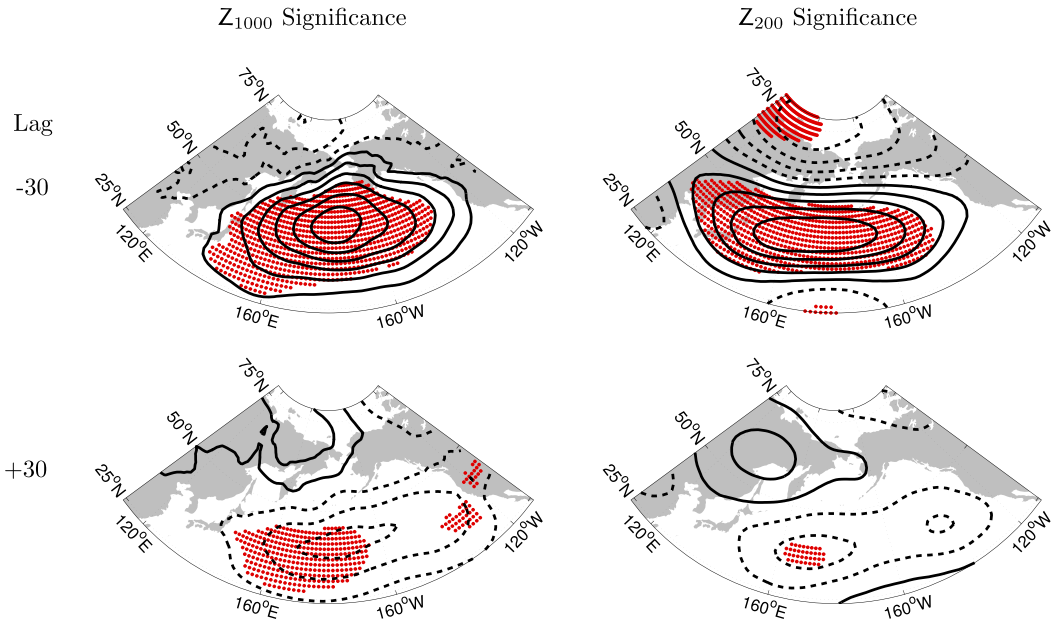


FIG. 4. Statistical significance of the (left) $Z_{1000}$ and (right) $Z_{200}$ anomalies at a lag of (top) −30 days and (bottom) +30 days. Regressions are shown in contours, and stippling indicates significance at the 95% confidence level using the two-tailed Student's $t$ test. Degrees of freedom are calculated per Eq. (31) from Bretherton et al. (1999).

(hereinafter $K_{\mathrm{ATMO}}$) was created by calculating the cosine-weighted average of daily-mean SLP anomalies over the region 39°–54°N, 150°E–171°W (i.e., near the center of action of the SLP anomalies in the lag −30 regression map in Fig. 2) for all days 1979–2013 and then standardizing the resulting index. By construction, the $K_{\mathrm{ATMO}}$ index indicates the temporal evolution of the anomalous atmospheric circulation observed at negative lags (top-left panels of Fig. 2) that does not depend on (direct) information from the SST field. To compare against the results based on the $K_{\mathrm{SST}}$ index, we regressed SST and SLP onto $K_{\mathrm{ATMO}}$ at 15-day intervals for lags spanning 0 to +60 days. Hence, lags of 0, +15, +30, +45, and +60 days from the $K_{\mathrm{ATMO}}$ regressions directly correspond to lags of −30, −15, 0, +15, and +30 days from the $K_{\mathrm{SST}}$ regressions, respectively.

The lag regressions of SST and SLP onto $K_{\mathrm{ATMO}}$ are shown in Fig. 6. The results indicate that the $K_{\mathrm{ATMO}}$ index projects onto SST anomalies over the KOE region, as expected from results based on the $K_{\mathrm{SST}}$ index (Fig. 2). The results also indicate that the SLP anomalies associated with the atmospheric index decay quickly over a time period of a few weeks, in contrast to the persistence of the atmospheric forcing pattern associated with the SST index (Fig. 2, left column). The shorter persistence of the atmospheric anomalies in Fig. 6 is consistent with the fact that the basis of the regression in Fig. 6 ($K_{\mathrm{ATMO}}$) has much more power on daily time scales than the basis of the regression in Fig. 2 ($K_{\mathrm{SST}}$). More importantly, the circulation anomalies associated with $K_{\mathrm{ATMO}}$ (Fig. 6) do *not* evolve into the pattern of SLP anomalies that lag the $K_{\mathrm{SST}}$ index. Thus, the evolution of the atmospheric forcing pattern appears to be independent of the anomalous atmospheric circulation that forms approximately a month after peak KOE SST anomalies. The results suggest that the pattern of circulation anomalies found at positive lags in Fig. 2 derives from information unique to the SST field.

## 4. Comparison with results based on SST anomalies in the Gulf Stream extension

The observational results presented in this study indicate that there are two very different and independent patterns of atmospheric circulation anomalies that lead and lag variations in KOE SSTs in the North Pacific on daily-mean time scales. The first pattern, which leads the largest KOE SST anomalies by several weeks, is characterized by statistically significant high pressure anomalies that span much of the North Pacific basin, and is consistent with atmospheric forcing of the ocean—as evidenced by the inferred pattern of warm temperature advection in Fig. 2 (top left) and the positive (downward) surface turbulent heat flux anomalies in Fig. 3 (top). The second pattern, which lags the largest KOE SST anomalies by approximately a month, is characterized by statistically significant low pressure anomalies that overlie the positive SST anomalies. The latter

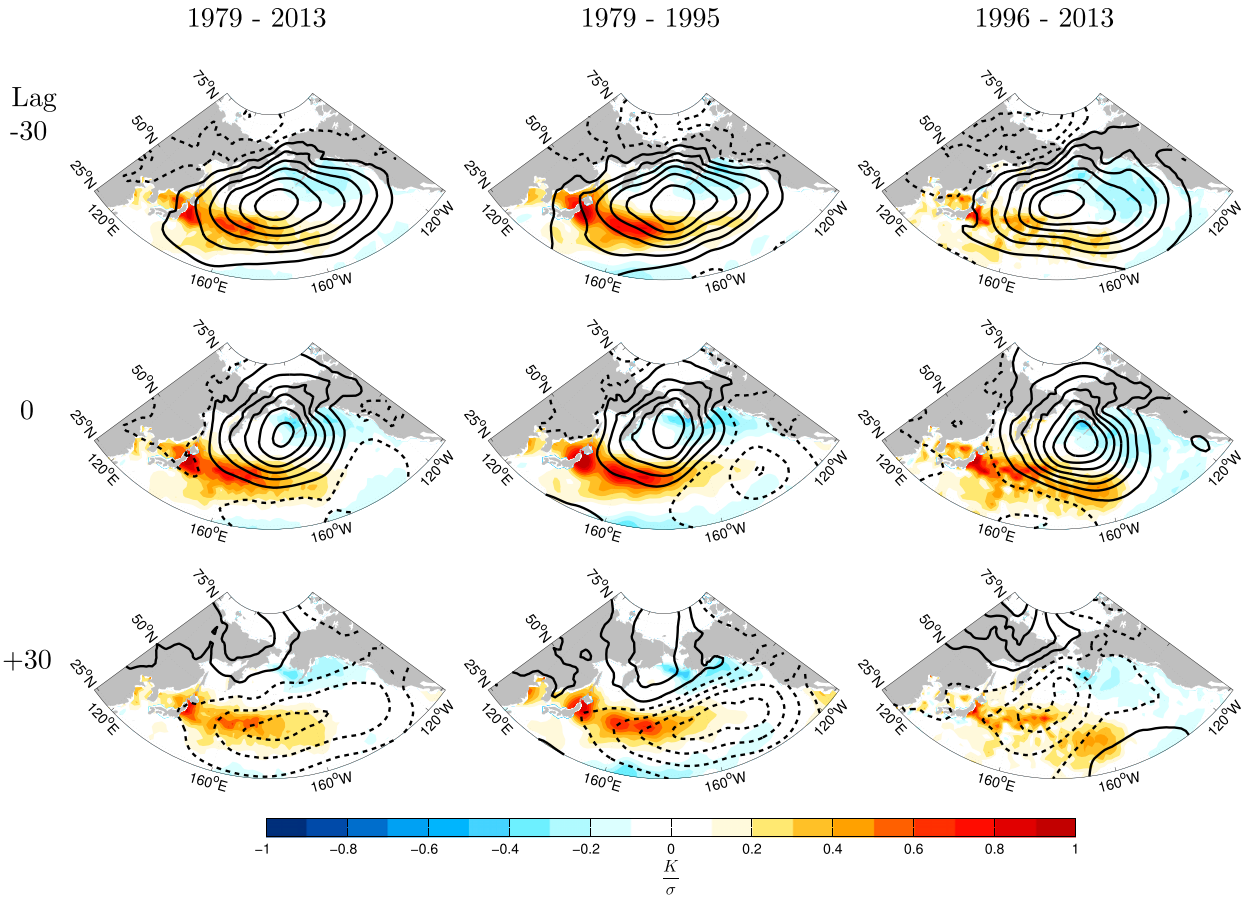


FIG. 5. As in the left column of Fig. 2, except the center and right columns show results of SST (shading) and $Z_{1000}$ (contours) regressed onto $K_{SST}$ for the ERA-Interim time periods of 1979–95 and 1996–2013, respectively.

pattern is marked by negative (upward) turbulent heat flux anomalies and is most robust at the surface. The observational results presented here are broadly similar to those found for SST anomalies in the Gulf Stream extension region in the companion paper Wills et al. (2016), as discussed in more detail below.

Figure 7 compares the SST and SLP fields regressed onto the $K_{SST}$ index used here (left) and the Gulf Stream extension index used in Wills et al. [(2016); see that study for details of the analysis] ($G_{SST}$; right). As in Fig. 2, lags span from −30 to +30 days, with negative lags indicating results where the SLP and SST fields precede peak amplitude in the SST index, and vice versa. In both the North Pacific and North Atlantic, positive SST anomalies in the western boundary current regions are preceded by circulation anomalies that are consistent with anomalous warm air advection over the western boundary current regions. The largest SST anomalies in each basin are of comparable amplitude and decay slowly over time. The circulation anomalies at negative lags are of similar magnitude and size and peak approximately 15–20 days prior to the strongest SST anomalies in both basins.

Importantly, the circulation anomalies at positive lag are also very similar over both ocean basins (bottom panels of Fig. 7). In particular, both basins exhibit anomalously low SLP centered approximately over the SST anomalies. High pressure anomalies are also found over each sector at positive lags, but the high pressure anomalies in the North Pacific are not significant (Fig. 4). *Hence, we view the anomalous low pressure pattern that develops over the SST anomalies to be the most robust common aspect of the atmospheric "response" over both ocean basins.*

## 5. Conclusions

In the current study and the companion paper by Wills et al. (2016), we investigated the observed daily-mean relationships between the atmospheric circulation and SST anomalies in the vicinity of the major Northern Hemisphere western boundary currents during the cold

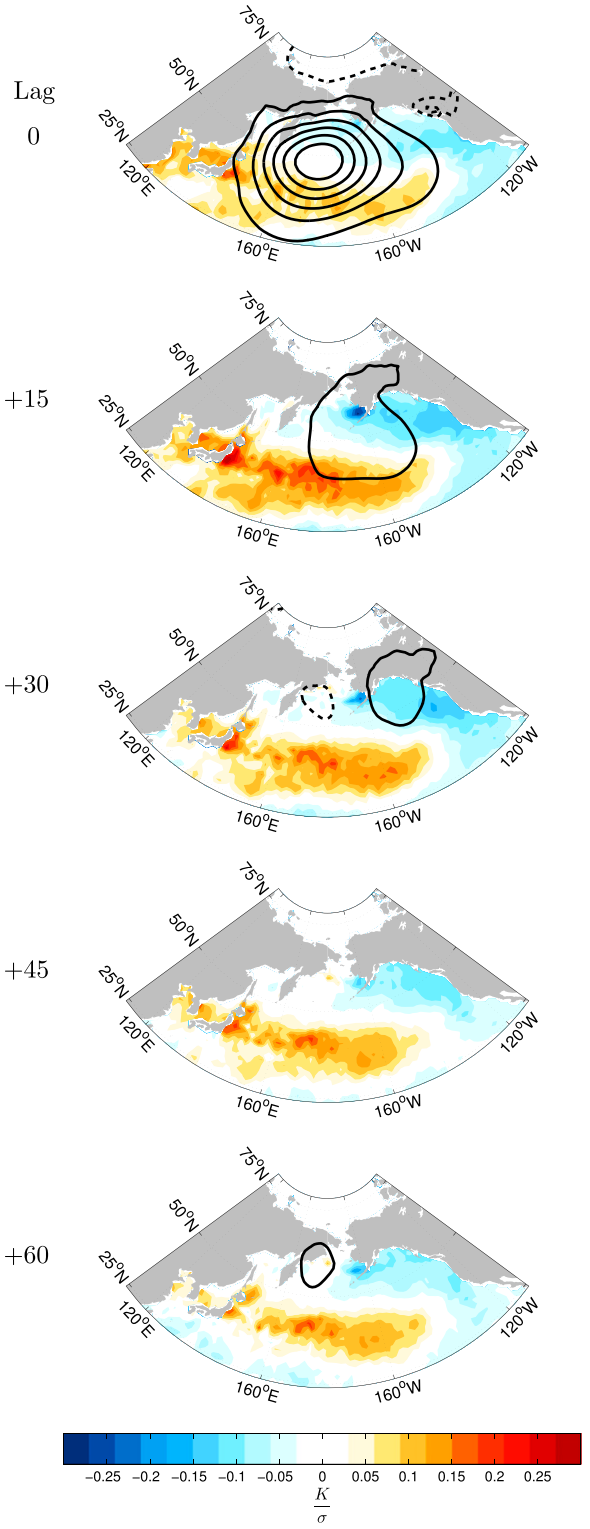


FIG. 6. Daily lag regressions of SST (shading) and $Z_{1000}$ (contours) onto the standardized $K_{ATMO}$ index. The $Z_{1000}$ contours with solid (dashed) lines represent positive (negative) values at an interval spacing of 15 m starting at ±7.5 m. Positive lags indicate the fields lagging the $K_{ATMO}$ index.

season. Together, the two studies suggest that SST anomalies in both the Gulf Stream and Kuroshio–Oyashio Extension regions are associated with distinct patterns of atmospheric variability that precede and follow peak amplitude in the SST field. Prior to the onset of peak SST anomalies, both basins exhibit similar "atmospheric forcing" patterns that are consistent with anomalous temperature advection due to the anomalous flow acting on the climatological-mean SST gradient. Following peak amplitude in the SST anomalies, both basins exhibit a distinct pattern of pressure anomalies centered over and to the east of the western boundary currents: warm SST anomalies are associated with low SLP anomalies that do not notably amplify with height. The most notable difference in the lagged patterns between the two ocean basins is the absence in the Pacific sector of significant high pressure anomalies to the north of the warm SST anomalies.

We hypothesize that the low surface pressure anomalies that lag SST anomalies in the western boundary currents reflect the "atmospheric response" to the SST field based on the following observations:

1) Results based on analyses over the Kuroshio–Oyashio and Gulf Stream Extension regions both yield very similar atmospheric "response" patterns during the weeks following peak SST anomalies in the western boundary currents (Fig. 7).
2) The response patterns have very different spatial structures than the "forcing" patterns that precede peak SST anomalies [Fig. 2 here and Fig. 2 from Wills et al. (2016)].
3) The response patterns are associated with negative (upward) surface turbulent heat flux anomalies, indicating that heat is being fluxed from the ocean surface to the overlying atmosphere as the SST anomalies decay (Fig. 3).
4) The response patterns are statistically significant over both ocean basins [Fig. 4 here and Fig. 3 from Wills et al. (2016)].
5) The response patterns do not emerge from analyses based on the evolution of the atmospheric circulation in the absence of (direct) information from the SST field [Fig. 6 here and Fig. 5 from Wills et al. (2016)].
6) The formation of low sea level pressure anomalies at a positive lag over and slightly east of warm SST anomalies is broadly consistent with the theoretical linear response to midlatitude SST anomalies (e.g., Hoskins and Karoly 1981).

The response pattern bears some resemblance to results from previous studies. Frankignoul et al. (2011) also found (weak) low pressure anomalies lagging warm SST anomalies in the KOE region by approximately one

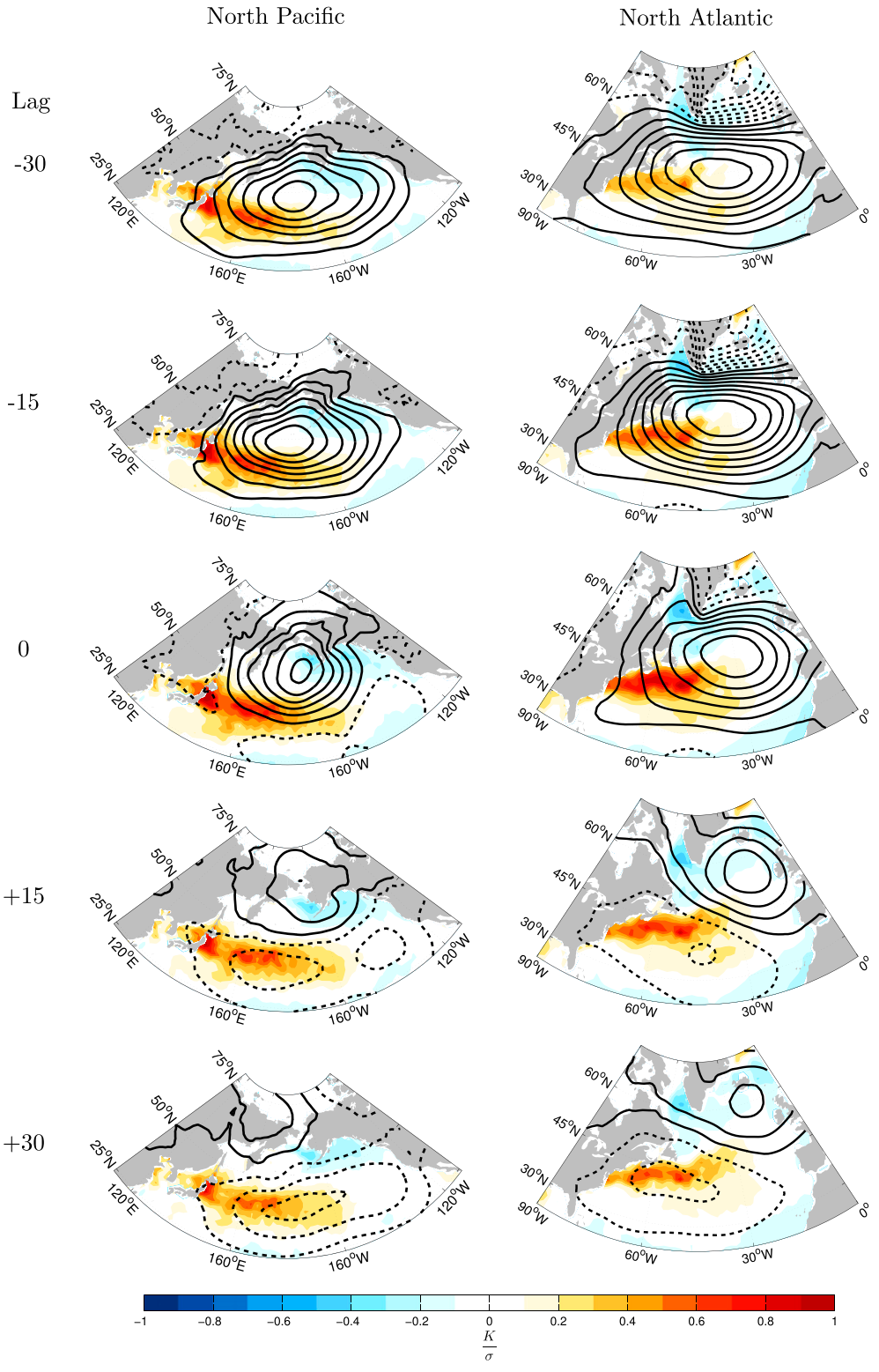


FIG. 7. Wintertime lag regressions of $Z_{1000}$ and SST onto the standardized (left) $K_{SST}$ index and (right) $G_{SST}$ index. Negative (positive) lags denote the $Z_{1000}$/SST anomalies leading (lagging) $K_{SST}$ and $G_{SST}$. The $Z_{1000}$ field is indicated by contours (spaced at 4-m intervals starting at $\pm 2$ m), where solid (dashed) lines indicate positive (negative) anomalies.

season in observational analyses based on lag regressions of a northward shift in the Kuroshio Extension. In addition to the low pressure anomalies, the authors found a significant equivalent barotropic high pressure centered over the northwestern North Pacific, similar to the pattern of (insignificant) high pressure anomalies found in the current study. Smirnov et al. (2015) found low pressure anomalies over the KOE region in numerical experiments forced with a realistic northward shift of the Oyashio Extension SST front in a low-resolution model, albeit the simulated response in their high-resolution model yielded enhanced ascent and much weaker low pressure anomalies over the KOE region. In observational analyses of decadal-scale variations in KOE SSTs, Taguchi et al. (2012) and Révelard et al. (2016) found that upward surface turbulent heat flux anomalies lagged warm SST anomalies by ~2 months, but their response patterns indicated robust high pressure anomalies near the Gulf of Alaska and the central and northwestern North Pacific, respectively.

Wintertime variations in SSTs in the Kuroshio–Oyashio Extension region are forced not only by variations in the surface turbulent heat fluxes—as emphasized here—but also by the ocean dynamical response to surface wind stress anomalies, variations in subtropical mode water (STMW) volume, changes in the path and transport of the western boundary current, anomalous oceanic temperature advection, remote teleconnections, and other factors (e.g., Kelly et al. 2010; Kwon et al. 2010; Frankignoul et al. 2011; Kwon and Joyce 2013; Smirnov et al. 2015). Hence, the results shown here have potential implications for understanding the atmospheric response to internal ocean dynamics in the Kuroshio–Oyashio Extension region.

It is important to note that the processes responsible for the formation of temporal SST anomalies differ between the Kuroshio–Oyashio and Gulf Stream regions. For example, the deeper thermocline in the Gulf Stream allows for larger quantities of heat storage in the STMW, while the shallower thermocline in the Kuroshio–Oyashio allows for wind-forced thermocline motion to impact heat storage (e.g., Kelly et al. 2010). On low-frequency time scales, wind-driven baroclinic Rossby waves can influence SST anomalies in both western boundary currents, but the impacts on the Gulf Stream are more limited given the relatively small size of the North Atlantic, the orientation of the Gulf Stream, and low-frequency interactions with the Atlantic meridional overturning circulation (e.g., Kwon et al. 2010). Nonetheless, our results suggest that there are very similar spatial and temporal relationships between atmospheric forcing and SST variability in both the Kuroshio–Oyashio and Gulf Stream Extensions on daily-mean time scales.

We plan to extend the analyses presented in this paper to examine and compare the observed relationships during the other seasons in a future follow-up study. We are currently designing numerical experiments that will explore the physical mechanisms of the responses indicated here in greater detail. The results of those experiments will be explored in a future paper.

*Acknowledgments.* The authors thank three anonymous reviewers for their detailed, constructive, and very helpful comments on the manuscript. SMW was funded by the NASA Physical Oceanography program under Grant NNX13AQ04G and the NSF Climate Dynamics program under grant AGS-1734251. DWJT was funded by the NASA Physical Oceanography program and the NSF Climate Dynamics program under Grant AGS-134080.

## REFERENCES

Alexander, M. A., 1992: Midlatitude atmosphere–ocean interaction during El Niño. Part I: The North Pacific Ocean. *J. Climate*, **5**, 944–958, https://doi.org/10.1175/1520-0442(1992)005<0944:MAIDEN>2.0.CO;2.

Barsugli, J. J., and D. S. Battisti, 1998: The basic effects of atmosphere–ocean thermal coupling on midlatitude variability. *J. Atmos. Sci.*, **55**, 477–493, https://doi.org/10.1175/1520-0469(1998)055<0477:TBEOAO>2.0.CO;2.

Brayshaw, D. J., B. Hoskins, and M. Blackburn, 2008: The storm-track response to idealized SST perturbations in an aqua-planet GCM. *J. Atmos. Sci.*, **65**, 2842–2860, https://doi.org/10.1175/2008JAS2657.1.

Bretherton, C. S., M. Widmann, V. P. Dymnikov, J. M. Wallace, and I. Bladé, 1999: The effective number of spatial degrees of freedom of a time-varying field. *J. Climate*, **12**, 1990–2009, https://doi.org/10.1175/1520-0442(1999)012<1990:TENOSD>2.0.CO;2.

Cayan, D. R., 1992: Latent and sensible heat flux anomalies over the northern oceans: Driving the sea surface temperature. *J. Phys. Oceanogr.*, **22**, 859–881, https://doi.org/10.1175/1520-0485(1992)022<0859:LASHFA>2.0.CO;2.

Chelton, D. B., and S.-P. Xie, 2010: Coupled ocean-atmosphere interaction at oceanic mesoscales. *Oceanography*, **23**, 52–69, https://doi.org/10.5670/oceanog.2010.05.

——, and Coauthors, 2001: Observations of coupling between surface wind stress and sea surface temperature in the eastern tropical Pacific. *J. Climate*, **14**, 1479–1498, https://doi.org/10.1175/1520-0442(2001)014<1479:OOCBSW>2.0.CO;2.

——, M. G. Schlax, M. H. Freilich, and R. F. Milliff, 2004: Satellite measurements reveal persistent small-scale features in ocean winds. *Science*, **303**, 978–983, https://doi.org/10.1126/science.1091901.

Ciasto, L. M., and D. W. J. Thompson, 2004: North Atlantic atmosphere–ocean interaction on intraseasonal time scales. *J. Climate*, **17**, 1617–1621, https://doi.org/10.1175/1520-0442(2004)017<1617:NAAIOI>2.0.CO;2.

Czaja, A., and N. Blunt, 2011: A new mechanism for ocean-atmosphere coupling in midlatitudes. *Quart. J. Roy. Meteor. Soc.*, **137**, 1095–1101, https://doi.org/10.1002/qj.814.

Davis, R. E., 1976: Predictability of sea surface temperature and sea level pressure anomalies over the North Pacific

Ocean. *J. Phys. Oceanogr.*, **6**, 249–266, https://doi.org/10.1175/1520-0485(1976)006<0249:POSSTA>2.0.CO;2.

——, 1978: Predictability of sea level pressure anomalies over the North Pacific Ocean. *J. Phys. Oceanogr.*, **8**, 233–246, https://doi.org/10.1175/1520-0485(1978)008<0233:POSLPA>2.0.CO;2.

Dee, D. P., and Coauthors, 2011: The ERA-Interim reanalysis: Configuration and performance of the data assimilation system. *Quart. J. Roy. Meteor. Soc.*, **137**, 553–597, https://doi.org/10.1002/qj.828.

Deser, C., and M. S. Timlin, 1997: Atmosphere–ocean interaction on weekly timescales in the North Atlantic and Pacific. *J. Climate*, **10**, 393–408, https://doi.org/10.1175/1520-0442(1997)010<0393:AOIOWT>2.0.CO;2.

Diaz, H. F., M. P. Hoerling, and J. K. Eischeid, 2001: ENSO variability, teleconnections and climate change. *Int. J. Climatol.*, **21**, 1845–1862, https://doi.org/10.1002/joc.631.

Frankignoul, C., N. Sennechael, Y.-O. Kwon, and M. A. Alexander, 2011: Influence of the meridional shifts of the Kuroshio and the Oyashio Extensions on the atmospheric circulation. *J. Climate*, **24**, 762–777, https://doi.org/10.1175/2010JCLI3731.1.

Hoskins, B. J., and D. J. Karoly, 1981: The steady linear response of a spherical atmosphere to thermal and orographic forcing. *J. Atmos. Sci.*, **38**, 1179–1196, https://doi.org/10.1175/1520-0469(1981)038<1179:TSLROA>2.0.CO;2.

Kelly, K. A., R. J. Small, R. M. Samelson, B. Qiu, T. M. Joyce, Y.- O. Kwon, and M. F. Cronin, 2010: Western boundary currents and frontal air–sea interaction: Gulf Stream and Kuroshio Extension. *J. Climate*, **23**, 5644–5667, https://doi.org/10.1175/2010JCLI3346.1.

Kushnir, Y., W. A. Robinson, I. Blade, N. M. J. Hall, S. Peng, and R. Sutton, 2002: Atmospheric GCM response to extratropical SST anomalies: Synthesis and evaluation. *J. Climate*, **15**, 2233–2256, https://doi.org/10.1175/1520-0442(2002)015<2233:AGRTES>2.0.CO;2.

Kwon, Y.-O., and T. M. Joyce, 2013: Northern Hemsiphere winter atmospheric transient eddy heat fluxes and the Gulf Stream and Kuroshio–Oyashio Extension variability. *J. Climate*, **26**, 9839–9859, https://doi.org/10.1175/JCLI-D-12-00647.1.

——, M. A. Alexander, N. A. Bond, C. Frankignoul, H. Nakamura, B. Qiu, and L. Thompson, 2010: Role of the Gulf Stream and Kuroshio–Oyashio systems in large-scale atmosphere-ocean interaction: A review. *J. Climate*, **23**, 3249–3281, https://doi.org/10.1175/2010JCLI3343.1.

Mantua, N. J., S. R. Hare, Y. Zhang, J. M. Wallace, and R. C. Francis, 1997: A Pacific interdecadal climate oscillation with impacts on salmon production. *Bull. Amer. Meteor. Soc.*, **78**, 1069–1079, https://doi.org/10.1175/1520-0477(1997)078<1069:APICOW>2.0.CO;2.

Masunaga, R., H. Nakamura, T. Miyasaka, K. Nishii, and Y. Tanimoto, 2015: Separation of climatological imprints of the Kuroshio Extension and Oyashio Fronts on the wintertime atmospheric boundary layer: Their sensitivity to SST resolution prescribed for atmospheric reanalysis. *J. Climate*, **28**, 1764–1787, https://doi.org/10.1175/JCLI-D-14-00314.1.

——, ——, ——, ——, and B. Qiu, 2016: Interannual modulations of oceanic imprints on the wintertime atmospheric boundary layer under the changing dynamical regimes of the Kuroshio Extension. *J. Climate*, **29**, 3273–3296, https://doi.org/10.1175/JCLI-D-15-0545.1.

Michel, C., and G. Rivieré, 2014: Sensitivity of the position and variability of the eddy-driven jet to different SST profiles in an aquaplanet general circulation model. *J. Atmos. Sci.*, **71**, 349–371, https://doi.org/10.1175/JAS-D-13-074.1.

Minobe, S., A. Kuwano-Yoshida, N. Komori, S.-P. Xie, and R. J. Small, 2008: Influence of the Gulf Stream on the troposphere. *Nature*, **452**, 206–210, https://doi.org/10.1038/nature06690.

——, M. Miyashita, A. Kuwano-Yoshida, H. Tokinaga, and S.- P. Xie, 2010: Atmospheric response to the Gulf Stream: Seasonal variations. *J. Climate*, **23**, 3699–3719, https://doi.org/10.1175/2010JCLI3359.1.

Nakamura, M., and S. Yamane, 2010: Dominant anomaly patterns in the near-surface baroclinicity and accompanying anomalies in the atmosphere and oceans. Part II: North Pacific basin. *J. Climate*, **23**, 6445–6467, https://doi.org/10.1175/2010JCLI3017.1.

Nakamura, H., T. Sampe, A. Goto, W. Ohfuchi, and S.-P. Xie, 2008: On the importance of midlatitude oceanic frontal zones for the mean state and dominant variability in the tropospheric circulation. *Geophys. Res. Lett.*, **35**, L15709, https://doi.org/10.1029/2008GL034010.

Newman, M., and Coauthors, 2016: The Pacific decadal oscillation, revisited. *J. Climate*, **29**, 4399–4427, https://doi.org/10.1175/JCLI-D-15-0508.1.

Nonaka, M., and S.-P. Xie, 2003: Covariations of sea surface temperature and wind over the Kuroshio and its extension: Evidence for ocean-to-atmosphere feedback. *J. Climate*, **16**, 1404–1413, https://doi.org/10.1175/1520-0442(2003)16<1404:COSSTA>2.0.CO;2.

O'Neill, L. W., D. B. Chelton, and S. K. Esbensen, 2003: Observations of SST-induced perturbations of the wind stress field over the Southern Ocean on seasonal timescales. *J. Climate*, **16**, 2340–2354, https://doi.org/10.1175/2780.1.

O'Reilly, C. H., and A. Czaja, 2015: The response of the Pacific storm track and atmospheric circulation to Kuroshio Extension variability. *Quart. J. Roy. Meteor. Soc.*, **141**, 52–66, https://doi.org/10.1002/qj.2334.

Palmer, T. N., and Z. Sun, 1985: A modelling and observational study of the relationship between sea surface temperature in the north-west Atlantic and the atmospheric general circulation. *Quart. J. Roy. Meteor. Soc.*, **111**, 947–975, https://doi.org/10.1002/qj.49711147003.

Piazza, M., L. Terray, J. Boé, E. Maisonnave, and E. Sanchez-Gomez, 2016: Influence of small-scale North Atlantic sea surface temperature patterns on the marine boundary layer and free troposphere: A study using the atmospheric ARPEGE model. *Climate Dyn.*, **46**, 1699–1717, https://doi.org/10.1007/s00382-015-2669-z.

Révelard, A., C. Frankignoul, and N. Sennéchael, 2016: Influence of the decadal variability of the Kuroshio Extension on the atmospheric circulation in the cold season. *J. Climate*, **29**, 2123–2144, https://doi.org/10.1175/JCLI-D-15-0511.1.

Sampe, T., H. Nakamura, A. Goto, and W. Ohfuchi, 2010: Significance of a midlatitude SST frontal zone in the formation of a storm track and an eddy-driven westerly jet. *J. Climate*, **23**, 1793–1814, https://doi.org/10.1175/2009JCLI3163.1.

Sheldon, L., and A. Czaja, 2014: Seasonal and interannual variability of an index of deep atmospheric convection over western boundary currents. *Quart. J. Roy. Meteor. Soc.*, **140**, 22–30, https://doi.org/10.1002/qj.2103.

Small, R. J., R. A. Tomas, and F. O. Bryan, 2014: Storm track response to ocean fronts in a global high-resolution climate model. *Climate Dyn.*, **43**, 805–828, https://doi.org/10.1007/s00382-013-1980-9.

Smirnov, D., M. Newman, and M. A. Alexander, 2014: Investigating the role of ocean–atmosphere coupling in the North Pacific Ocean. *J. Climate*, **27**, 592–606, https://doi.org/10.1175/JCLI-D-13-00123.1.

——, ——, ——, Y.-O. Kwon, and C. Frankignoul, 2015: Investigating the local atmospheric response to a realistic shift in

the Oyashio sea surface temperature front. *J. Climate*, **28**, 1126–1147, https://doi.org/10.1175/JCLI-D-14-00285.1.

Sugimoto, S., 2014: Influence of SST anomalies on winter turbulent heat fluxes in the eastern Kuroshio–Oyashio confluence region. *J. Climate*, **27**, 9349–9358, https://doi.org/10.1175/JCLI-D-14-00195.1.

——, and K. Hanawa, 2011: Roles of SST anomalies on the wintertime turbulent heat fluxes in the Kuroshio–Oyashio confluence region: Influences of warm eddies detached from the Kuroshio Extension. *J. Climate*, **24**, 6551–6561, https://doi.org/10.1175/2011JCLI4023.1.

Taguchi, B., H. Nakamura, M. Nonaka, N. Komori, A. Kuwano-Yoshida, K. Takaya, and A. Goto, 2012: Seasonal evolutions of atmospheric response to decadal SST anomalies in the North Pacific subarctic frontal zone: Observations and a coupled model simulation. *J. Climate*, **25**, 111–139, https://doi.org/10.1175/JCLI-D-11-00046.1.

Wills, S. M., D. W. J. Thompson, and L. M. Ciasto, 2016: On the observed relationships between variability in Gulf Stream sea surface temperatures and the atmospheric circulation over the North Atlantic. *J. Climate*, **29**, 3719–3730, https://doi.org/10.1175/JCLI-D-15-0820.1.